Statistics of the stochastically forced Lorenz attractor by the Fokker-Planck equation and cumulant expansions

Altan Allawala[*] and J. B. Marston[†]
Department of Physics, Box 1843, Brown University, Providence, Rhode Island 02912-1893, USA
(Received 7 April 2016; revised manuscript received 18 October 2016; published 23 November 2016)

We investigate the Fokker-Planck description of the equal-time statistics of the three-dimensional Lorenz attractor with additive white noise. The invariant measure is found by computing the zero (or null) mode of the linear Fokker-Planck operator as a problem of sparse linear algebra. Two variants are studied: a self-adjoint construction of the linear operator and the replacement of diffusion with hyperdiffusion. We also access the low-order statistics of the system by a perturbative expansion in equal-time cumulants. A comparison is made to statistics obtained by the standard approach of accumulation via direct numerical simulation. Theoretical and computational aspects of the Fokker-Planck and cumulant expansion methods are discussed.

DOI: 10.1103/PhysRevE.94.052218

I. INTRODUCTION

Chaotic dynamical systems often have a well-defined statistical steady state. Traditionally statistics are estimated by their accumulation through direct numerical simulation (DNS) starting from an ensemble of initial conditions. If the basin of attraction is ergodic, ensemble averaging can be replaced by time averaging over a single long trajectory. Rare but large deviations may occur, however, necessitating extremely long integration times. An alternative and more efficient approach solves for the statistics directly. Depending on the question to be answered, such direct statistical simulation (DSS) can focus on various statistical quantities such as the probability distribution function (PDF) or invariant measure, the low-order equal-time moments, autocorrelations in time, or large deviations.

This paper presents two different types of DSS. The first, the Fokker-Planck equation (FPE), describes the flow of probability density in phase space, respecting the conservation of total probability. Consider a trajectory governed by the differential equation

$$\frac{d\vec{x}}{dt} = \vec{V}(\vec{x}) + \vec{\eta}(t), \tag{1}$$

where $\vec{\eta}(t)$ is additive stochastic forcing. The FPE for this system is

$$\frac{\partial P(\vec{x},t)}{\partial t} = -\hat{L}_{\rm FPE} P(\vec{x},t), \tag{2}$$

where we will call $\hat{L}_{\rm FPE}$ the (linear) FPE operator. The placement of the negative sign in front of the operator $\hat{L}_{\rm FPE}$ in Eq. (2) is for convenience: The operator $\hat{L}_{\rm FPE}$ is then semipositive definite and the steady-state statistics are determined by the ground state. In the special case where $\vec{\eta}$ is Gaussian additive white noise with no mean and covariance given by

$$\langle \eta_i(t)\eta_j(t')\rangle = 2\Gamma_{ij}\delta(t-t'), \tag{3}$$

with angular brackets indicating a short time average, only a finite number of terms appear in the FPE operator [1]:

$$\hat{L}_{\rm FPE} P = \vec{\nabla}\cdot(\vec{V}P) - \Gamma\nabla^2 P. \tag{4}$$

Additive stochastic forcing smears out the PDF P through diffusion in phase space. A canonical example is the one-dimensional Ornstein-Uhlenbeck process with trajectories governed by

$$\dot{x} = -ax + \eta(t). \tag{5}$$

The corresponding FPE is

$$\frac{\partial P(x,t)}{\partial t} = \frac{\partial}{\partial x}[ax P(x,t)] + \Gamma\frac{\partial^2 P(x,t)}{\partial x^2}, \tag{6}$$

which has a steady-state solution that is readily found to be Gaussian:

$$P(x) = \sqrt{\frac{a}{2\pi\Gamma}}e^{-ax^2/2\Gamma}. \tag{7}$$

As we will see, stochastic forcing also needs to be introduced to regulate strange attractors at small scales. As the fractal structure of a strange attractor cannot be resolved on a lattice, it is necessary to smooth the structure at the lattice length scale. We use additive stochastic forcing for this purpose.

Direct solution of the FPE is most commonly carried out for one-dimensional systems. Extension to higher dimensions is conceptually straightforward, but numerically challenging [2]. The objective of the present paper is to apply the FPE to a three-dimensional chaotic system. Numerical solutions have been developed based on finite elements [3,4], finite differences [5], and path integrals [6]. Here we depart from these traditional methods by instead directly solving for the zero or null mode of a finite-difference discretized FPE operator, thus obviating the time-consuming and costly steps of computing the transient probability distributions. We illustrate this method by applying it to the Lorenz system [7] with additive stochastic forcing. Although a phenomenological FPE has been applied for a quantum system without the addition of stochastic forcing [8], we follow previous work [9–13] and add small additive white noise to wash out fractal structure below the lattice scale.

Since numerical solution of the FPE in larger numbers of dimensions is stymied by the "curse of dimensionality," it is

[*]allawala@brown.edu
[†]marston@brown.edu

important to develop alternative forms of DSS. Accordingly, we also explore a second type of DSS, an expansion in equal-time cumulants that can be applied to high-dimensional dynamical systems. A cumulant expansion was employed for the Orszag-McLaughlin attractor in Ref. [14]. For the Lorenz attractor we show that low-order statistics are well reproduced at third-order truncation.

The paper is organized as follows. Section II briefly describes the Lorenz system with additive stochastic forcing and its numerical integration. Two different sets of parameters are considered, both of which yield chaotic behavior. Section III describes the FPE and the numerical method that we use to find the invariant measure. Equal-time statistics so obtained are compared to those found through accumulation by DNS. We study the scaling of the spectral gap of the linear FPE operator as the stochastic forcing is varied. Two extensions to the method are also considered: a self-adjoint construction of the linear operator and the replacement of diffusion with hyperdiffusion. Section IV presents the cumulant expansion technique and its evaluation by comparison to DNS. A summary is presented in Sec. V.

II. LORENZ ATTRACTOR WITH ADDITIVE STOCHASTIC FORCING

The Lorenz attractor is a three-dimensional chaotic system that was originally derived by applying a severe Galerkin approximation to the equations of motion (EOMs) for Rayleigh-Bénard convection with stress-free boundary conditions [7]. We study an extension with additive stochastic forcing [9–13] that obeys Eq. (3). Such additive white noise can model fast or unresolved physical processes that are not explicitly described,

$$\begin{aligned}\dot{x} &= \sigma(y-x)+\eta_1(t),\\ \dot{y} &= x(\rho-z)-y+\eta_2(t),\\ \dot{z} &= xy-\beta z+\eta_3(t).\end{aligned} \tag{8}$$

In this context x is proportional to convective intensity, y to the difference in temperature between ascending and descending currents, and z to the vertical temperature profile's deviation from linearity. The parameters β, ρ, and σ are a geometric factor, the Rayleigh number, and the Prandtl number, respectively. We also choose the covariance of the Gaussian white noise to be diagonal and isotropic: $\Gamma_{ij}=\Gamma\delta_{ij}$.

We study the strange attractor at two different sets of parameters. The conventional (classic) parameters are $\beta=1.0$, $\rho=26.5$, and $\sigma=3.0$. We also examine the case with the geometric factor changed to $\beta=0.16$. This modification enhances layering in the PDF. Since the geometric factor is related to the size of the attractor, a reduction in β shrinks the attractor, which in turn allows for a reduction in the stochastic forcing while keeping the structure sufficiently smooth at the lattice length scale. The attractors have two prominent wings (see Fig. 1). Transitions between the two wings are characterized by a long time scale, whereas orbits within each wing occur on a fast time scale of order $\tau\approx 1$.

Direct numerical simulation

The EOMs (8) are integrated forward in time with the fourth-order accurate Runge-Kutta algorithm with fixed time step $\delta t=0.01$. Stochastic forcing, drawn from a normal distribution, is updated at intervals of $\Delta t=0.1$ and interpolated at intermediate times δt. Note that there is a good separation of time scales with $\tau\gg\Delta t\gg\delta t$ following the reasoning of Ref. [15].

Statistics are accumulated up to a final time $T=2\times10^7$. The PDF is estimated from the histogram that results from binning the trajectory into cubic boxes. The PDF is projected onto a plane by integrating over the direction perpendicular to the plane, for instance,

$$P(x,y)=\int_{-\infty}^{\infty}P(x,y,z)dz. \tag{9}$$

Figures 1, 3, and 5 show that even small stochastic forcing smoothes out the fine structure of the strange attractor [16]; in particular, the ringlike steps in the PDF disappear.

III. FOKKER-PLANCK EQUATION

The FPE is an attractive alternative to the accumulation of statistics by DNS. The linear FPE operator for the Lorenz system

$$\begin{aligned}\hat{L}_{\rm FPE}P=\vec{\nabla}\cdot\{[\sigma(y-x),&x(\rho-z)\\ &-y,xy-\beta z]P]\}-\Gamma\nabla^2P\end{aligned} \tag{10}$$

is positive-definite in the sense that the real part of the eigenvalues are non-negative [if that were not the case, Eq. (2) would diverge]. The equal-time PDF of the FPE is the zero or null mode of $\hat{L}_{\rm FPE}$. By discretizing the operator on a lattice, the problem of finding the zero mode is converted to a problem of sparse linear algebra.

A. Numerical solution

A standard center-difference scheme is used to discretize the derivatives that appear in Eq. (10):

$$\begin{aligned}f_i' &\approx \frac{f_{i+1}-f_{i-1}}{2\Delta x},\\ f_i'' &\approx \frac{f_{i+1}-2f_i+f_{i-1}}{\Delta x^2}.\end{aligned} \tag{11}$$

The PDF of the unforced Lorenz attractor has compact support, but once stochastic forcing is included the PDF is nonzero but exponentially small throughout phase space. In the numerical calculation, the probability density P is taken to vanish outside of the domain. The zero mode of $\hat{L}_{\rm FPE}$ is found with the use of a preconditioned Jacobi-Davidson QR (JDQR) algorithm [17,18] that computes the partial Schur decomposition of a matrix with error tolerance set to 10^{-5}. We have checked that our results do not change appreciably for tighter tolerances. Although the JDQR algorithm is well suited for sparse matrices, requiring only the action of a matrix multiplying a vector, we were unable to find a suitable sparse preconditioner. A sparse preconditioner would enable a substantial increase in resolution. The Jacobi correction equation is preconditioned following Sec. 3.2 of Ref. [18] and solved using the generalized minimal residual method using MATLAB. The highest resolution we have been able to reach is 160^3 with 500 GB of memory. This large number of grid points for which the Fokker-Planck equation has been

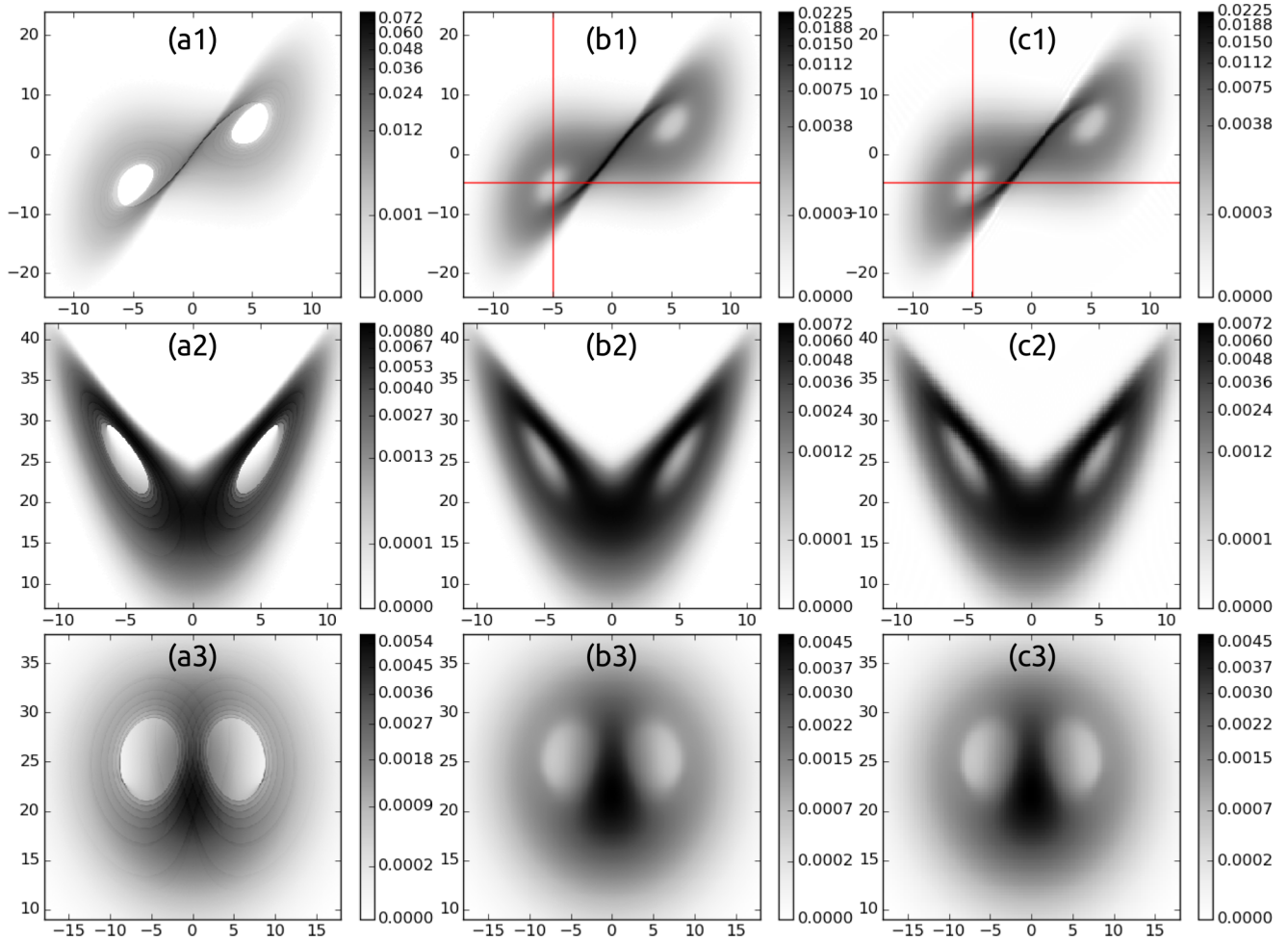

FIG. 1. (a) PDF of the unforced Lorenz system (binned on a 637^3 grid) accumulated by DNS. Classic Lorenz parameters are used (see Sec. II). (b) Same as (a), but with added stochastic forcing ($\Gamma = 0.2$) (478^3 grid). Note that the fine rings visible in the unforced system are washed out by the noise. (c) PDF of the stochastically forced attractor ($\Gamma = 0.2$) as obtained from the zero mode of $\hat{L}_{\mathrm{FPE}}$ on a 160^3 grid and for $x \in [-12.5, 12.5]$, $y \in [-24, 24]$, and $z \in [1, 45]$. The JDQR algorithm is employed. Rows (1), (2), and (3) correspond to the x-y, x-z, and y-z projections of the PDF, respectively. Good agreement between (b) DNS and (c) FPE is evident. Red lines correspond to the cross sections shown in Fig. 2.

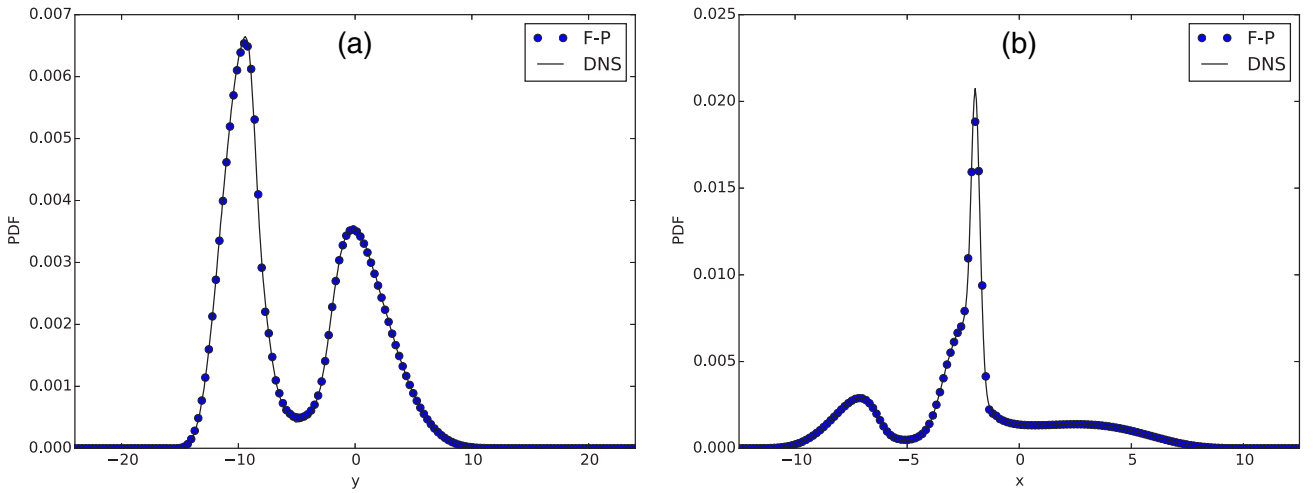

FIG. 2. (a) Vertical and (b) horizontal slices along the red lines of the x-y planar projection shown in Fig. 1. The DNS and FPE methods agree quantitatively.

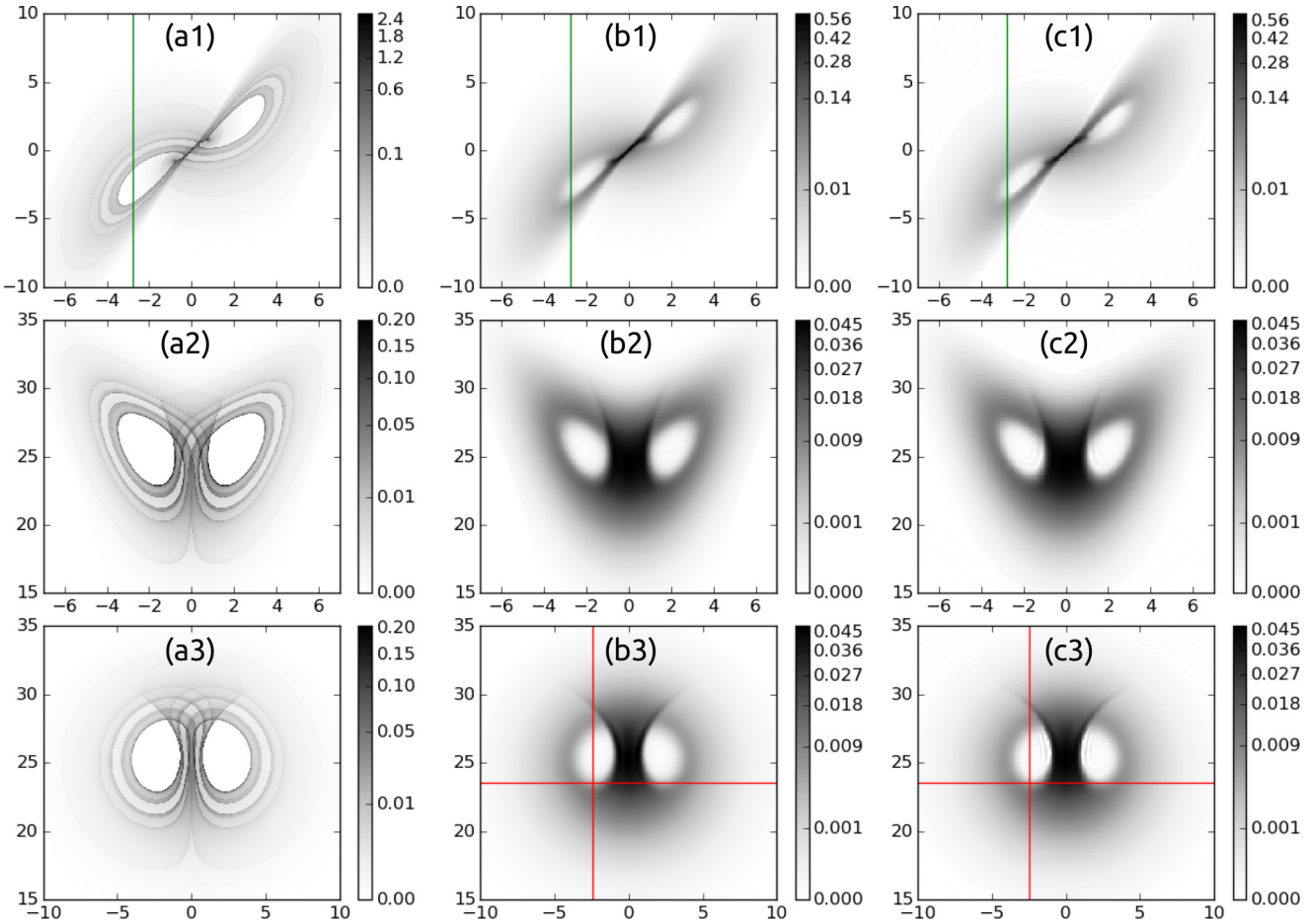

FIG. 3. (a) PDF of the unforced Lorenz system (binned on a 637^3 grid) accumulated by DNS. Modified parameters are used (see Sec. II). (b) Same as (a), but with added stochastic forcing ($\Gamma = 0.02$) (478^3 grid). Note that the fine rings visible in the unforced system are washed out by the noise. (c) PDF of the stochastically forced attractor ($\Gamma = 0.02$) as obtained from the zero mode of $\hat{L}_{\mathrm{FPE}}$ on a 160^3 grid and for $x \in [-7,7]$, $y \in [-10,10]$, and $z \in [15,35]$. Rows (1), (2), and (3) correspond to the x-y, x-z, and y-z projections of the PDF, respectively. Good agreement between (b) DNS and (c) FPE is evident. Red lines correspond to the cross sections shown in Fig. 4 and green lines correspond to the cross section shown in Fig. 5.

simulated is more than double the number reached by Kumar and Narayanan [5]. This is made possible by reexpressing the time-dependant Fokker-Planck problem as a sparse linear algebra problem. On the 160^3 grid, the $\hat{L}_{\mathrm{FPE}}$ matrix has 28 518 400 nonzero elements and a sparsity of 1.70×10^{-6}.

Modes at the maximal wave number decay diffusively due to the stochastic forcing with a decay time scale τ_d given by

$$\tau_d^{-1} = \frac{\pi^2 \Gamma}{4}[(\Delta x)^{-2} + (\Delta y)^{-2} + (\Delta z)^{-2}]. \qquad (12)$$

Equating this time scale to the time scale of fast dynamics τ provides an estimate of the effective resolution of the discretized FPE.

Figures 1–5 show good quantitative agreement between PDFs accumulated by DNS and those obtained from the zero mode of the FPE operator. The fine structure evident in the x-z and y-z projections of the PDF for the Lorenz attractor with modified parameters (Fig. 3) is reproduced by the FPE. The modified parameters also demonstrate the sensitivity of the fractal structure to stochastic forcing. Even forcing as small as $\Gamma = 0.02$ washes out the ringlike steps in the PDF in Fig. 3, also shown by the selected horizonal slice in Fig. 5.

B. Eigenvalue spectra of the Fokker-Planck operator

The gap to the eigenmode with the smallest nonzero real part of its eigenvalue is of interest as it corresponds to the slowest relaxation rate in the statistics towards the statistical steady state. Likewise, the imaginary components of the eigenvalues of the linear FPE operator set the quasiperiodic frequency of the dynamical system (see Sec. II for a discussion of the slow and fast time scales). This interpretation of the real and imaginary components of the eigenvalues can be illustrated analytically with a two-dimensional linear Ornstein-Uhlenbeck system with circular orbits of period 2π that decay at rate α:

$$\dot{x} = y - \alpha x + \eta_1(t),$$
$$\dot{y} = -x - \alpha y + \eta_2(t). \qquad (13)$$

The eigenvalues of the FPE operator of this system are $\lambda_{n,m} = \alpha n \pm im$, where m and n are non-negative integers that are either both odd or both even and $m \leqslant n$. [The eigenvalues

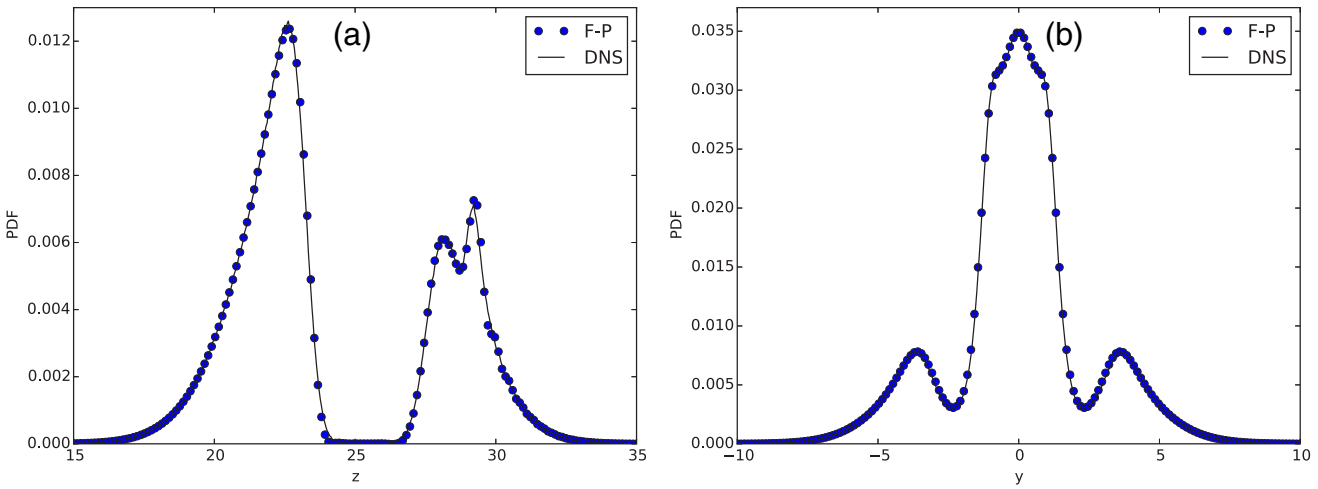

FIG. 4. (a) Vertical and (b) horizontal slices along the red lines of the y-z planar projection shown in Fig. 3. The DNS and FPE methods agree quantitatively.

can be found by transforming to polar coordinates and expressing the PDF as a separable solution $P(r,\theta) = R(r)\Theta(\theta)$ with the radial equation solved using generalized Laguerre polynomials.] Because the system of Eq. (13) is linear, the stochastic forcing does not affect the spectra. The real parts of the eigenvalues are determined by the decay rate α, whereas the imaginary part is set by the orbital period.

The spectrum of low-lying eigenvalues is shown in Fig. 6 with the complex eigenvalues appearing in conjugate pairs because $\hat{L}_{\mathrm{FPE}}$ is purely real valued. Increased stochastic forcing increases the values of the real components of the eigenvalues of the FPE operator, in turn shortening the relaxation time scale. Linear extrapolation to the unforced ($\Gamma = 0$) limit yields a real eigenvalue of 0.0802 corresponding to a relaxation time scale of about 12, in accord with expectations. Likewise, the nonzero imaginary parts of the eigenvalues in Fig. 6 correspond to the oscillation frequency around each of the two wings of the Lorenz attractor as well as the slower rate of transitions between the two wings.

C. Extensions

We consider two modifications to the FPE operator. Self-adjoint constructions of the linear operator are considered first and then the replacement of diffusion with hyperdiffusion.

1. Self-adjoint linear FPE operators

We investigate whether or not self-adjoint generalizations of the linear FPE operator have any advantages. One way to construct such an operator is to double the size of the linear

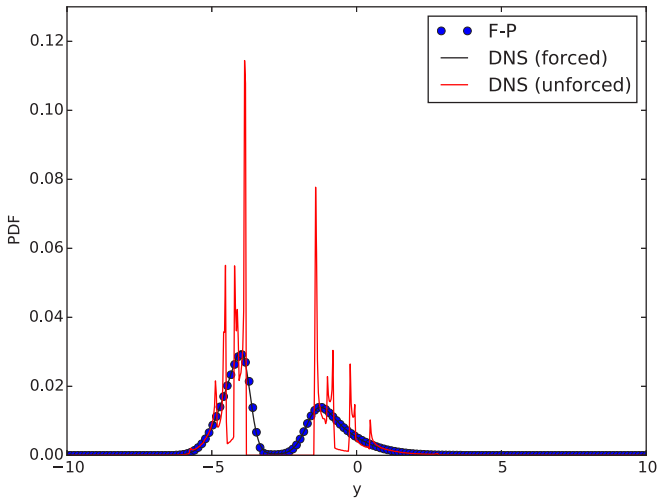

FIG. 5. Cross section through the x-y planar projection of the PDF where $x = -2.77$ for unforced DNS, stochastically forced DNS, and a stochastically forced FPE (with $\Gamma = 0.02$). Modified parameters are used. Sharp peaks in probability seen in the unforced Lorenz system are eliminated by the stochastic forcing.

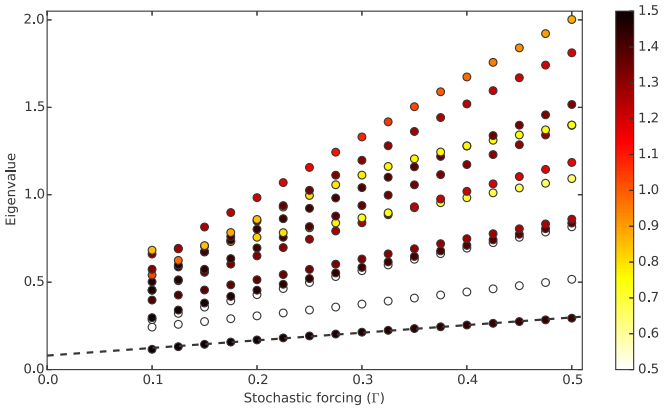

FIG. 6. Real component of the first 12 nonzero eigenvalues of the linear FPE operator of the Lorenz system (on an 80^3 lattice grid) as a function of stochastic forcing Γ. Modified parameters are used (see Sec. II) with $x \in [-12.5,12.5]$, $y \in [-17.5,17.5]$, and $z \in [7.5,42.5]$. The phase of each eigenvalue is represented by the color of the points, with white corresponding to a phase of zero. A linear extrapolation of the first nonzero eigenvalue to $\Gamma = 0$ is shown. The second and third nonzero eigenvalues are purely real.

space by introducing the operator

$$\hat{H}_2 = \begin{pmatrix} 0 & \hat{L}_{\rm FPE} \\ \hat{L}^\dagger_{\rm FPE} & 0 \end{pmatrix} \tag{14}$$

that by construction obeys $\hat{H}_2^\dagger = \hat{H}_2$. Here $\hat{H}_2$ is no longer positive-definite; instead its eigenvalue spectrum is symmetric about 0. Finding the zero mode therefore requires a numerical algorithm that can target the middle of the spectrum. Alternatively, the operator

$$\hat{H}_1 \equiv \hat{L}^\dagger_{\rm FPE}\hat{L}_{\rm FPE} \tag{15}$$

is self-adjoint, positive-definite, and has the same ground state as $\hat{L}_{\rm FPE}$. To see this define $|V\rangle \equiv \hat{L}_{\rm FPE}|\Psi_0\rangle$, where $|\Psi_0\rangle$ is the zero mode of $\hat{H}_1$. Then $\langle\Psi_0|\hat{L}^\dagger_{\rm FPE}\hat{L}_{\rm FPE}|\Psi_0\rangle = \langle V|V\rangle = 0$, which implies that $|V\rangle$ must have zero norm $|V\rangle = |0\rangle$, and $|\Psi_0\rangle$ is the zero mode of $\hat{L}_{\rm FPE}$. The ground state of a quantum system has (under rather general conditions) no nodes, so $\Psi_0(\vec{x})$ automatically produces a non-negative PDF, an added virtue of viewing steady-state solutions of the FPE as a problem of linear algebra.

Because the ground state of $\hat{H}_1$ might possibly be found using simulated annealing or quantum annealing and adiabatic quantum computation [19,20], it is of interest to investigate its numerical solution. A drawback of $\hat{H}_1$ is that the eigenvalues are clustered more tightly around 0 than those of $\hat{L}$, slowing convergence. We find that the ground state, computed using the Davidson algorithm [21,22], matches that obtained from $\hat{L}_{\rm FPE}$ alone.

2. *Hyperdiffusion*

Another interesting variant to investigate is to replace diffusion in Eq. (10) with biharmonic hyperdiffusion:

$$-\Gamma\nabla^2 \to \Gamma_2\nabla^4. \tag{16}$$

As hyperdiffusion is more scale selective than ordinary diffusion, it acts to smooth out structure at the lattice scale while leaving larger structures intact. Holding the dissipation rate at the lattice scale fixed, Γ_2 scales inversely with the fourth power of the spacing [contrast with Eq. (12)]. Unlike ordinary diffusion that has a physical origin in stochastic forcing, hyperdiffusion violates realizability, leading to negative probability densities (see, for example, Sec. 4.3 of Ref. [23]). Also, hyperdiffusion reduces the sparseness of the discretized linear FPE operator, slowing computation. On an 80^3 grid the PDF shows less fine structure, as expected.

IV. CUMULANT EXPANSION

Numerical solution of the FPE for dynamical systems of dimension greater than 3 is increasingly difficult. Therefore, it is of interest to explore other approaches to DSS. Here we use an expansion in low-order equal-time cumulants to find the statistics of the Lorenz attractor. In addition to the Orszag-McLaughlin attractor [14], it has also been applied to a number of high-dimensional problems in fluids using spatial averaging [24–31], although sometimes ensemble averages are employed [32,33].

The EOMs for equal-time cumulants can be elegantly derived using the Hopf functional formalism [25,34]. However, it is also possible to derive them directly from the EOMs of the dynamical system. Consider a general system with quadratic nonlinearities

$$\dot{q}_i = F_i + L_{ij}q_j + Q_{ijk}q_jq_k + \eta_i. \tag{17}$$

A Reynolds decomposition

$$q_i = \overline{q_i} + q_i' \tag{18}$$

of the dynamical variables q_i into a mean and a fluctuation is the starting point. Here (and as discussed below) the average is chosen to be a mean over initial conditions drawn from a Gaussian distribution. The Reynolds decomposition obeys the rules

$$\begin{aligned} \overline{\overline{q_i}} &= \overline{q}_i, \\ \overline{q_i'} &= 0, \\ \overline{\overline{q}_i q_j} &= \overline{q}_i\overline{q}_j. \end{aligned} \tag{19}$$

The first cumulant c_i is the mean of q_i and the second and third cumulants are given by centered moments of the fluctuations. By contrast, the fourth cumulant is *not* a centered moment:

$$\begin{aligned} c_i &\equiv \overline{q_i}, \\ c_{ij} &\equiv \overline{q_i'q_j'}, \\ c_{ijk} &\equiv \overline{q_i'q_j'q_k'}, \\ c_{ijk\ell} &\equiv \overline{q_i'q_j'q_k'q_\ell'} - c_{ij}c_{k\ell} - c_{ik}c_{j\ell} - c_{i\ell}c_{jk}. \end{aligned} \tag{20}$$

These definitions ensure that the third and higher cumulants of a Gaussian distribution vanish.

The EOMs for the cumulants may be found directly. The equation of motion for the first cumulant is obtained by ensemble averaging Eq. (17) and using the definitions of the first and second cumulants in Eq. (20),

$$\begin{aligned} \frac{dc_i}{dt} &= \overline{\frac{dq_i}{dt}} \\ &= F_i + L_{ij}\overline{q_j} + Q_{ijk}\overline{q_jq_k} \\ &= F_i + L_{ij}c_j + Q_{ijk}(c_jc_k + c_{jk}). \end{aligned} \tag{21}$$

The tendency of the first cumulant involves the second cumulant. Truncating at first order by discarding the second cumulant, the CE1 approximation, shows that the first cumulant obeys the same EOMs as Eq. (17); hence there is no nontrivial fixed point solution. In general, for quadratically nonlinear systems the tendency of the nth cumulant requires knowledge of the $(n+1)$th cumulant, the well-known closure problem. Thus the EOM for the second cumulants requires the first, second, and third cumulants:

$$\begin{aligned} \frac{dc_{ij}}{dt} &= 2\left\{\overline{\frac{dq_i'}{dt}q_j'}\right\} \\ &= 2\left\{\overline{\left(\frac{dq_i}{dt} - \frac{d\overline{q_i}}{dt}\right)q_j'}\right\} \\ &= 2\left\{\overline{\frac{dq_i}{dt}q_j'}\right\} \end{aligned}$$

$$= 2\{\overline{L_{ik}q_k q'_j + Q_{ik\ell}q_k q_\ell q'_j}\} + 2\Gamma_{ij}$$
$$= \{2L_{ik}c_{kj} + Q_{ik\ell}(4c_k c_{\ell j} + 2c_{k\ell j})\} + 2\Gamma_{ij}. \quad (22)$$

The covariance matrix Γ_{ij} of the stochastic forcing appears in the last two lines as (implicitly) a short-time averaging has been carried out in addition to ensemble averaging. The symmetrization operation $\{\cdots\}$ over all permutations of the free indices has been introduced for conciseness. In the case of a two-index variable such as the second cumulant it is defined as $\{c_{ij}\} = \frac{1}{2}(c_{ij} + c_{ji})$ and similarly for higher cumulants.

Because each higher cumulant carries an additional dimension with it, closure should be performed as soon as possible. Closing the EOMs at second order by discarding the contribution of the third cumulant c_{ijk} (CE2) is sometimes possible [24] and yields a realizable approximation (because the PDF is Gaussian that is non-negative everywhere). The CE2 EOMs can then be integrated forward in time by specifying as an initial condition nonzero first and second cumulants, corresponding to a normally distributed initial ensemble. However, the Lorenz attractor is so nonlinear that the CE2 EOMs, integrated forward in time, do not reach a fixed point that would characterize a statistical steady state. Therefore, we proceed to next order, CE3, by setting the fourth cumulant to zero, $c_{ijkl} = 0$. The fourth centered moment may then be expressed in terms of the second and third cumulants

$$\overline{q'_m q'_n q'_j q'_k} = c_{mn}c_{jk} + c_{mj}c_{nk} + c_{mk}c_{jn} + c_{mnjk}$$
$$\simeq c_{mn}c_{jk} + c_{mj}c_{nk} + c_{mk}c_{jn} \quad \text{(CE3)} \quad (23)$$

and the EOM for the third cumulant now closes:

$$\frac{dc_{ijk}}{dt} = 3\left\{\overline{\frac{dq'_i}{dt}q'_j q'_k}\right\}$$
$$= 3\left\{\overline{\left(\frac{dq_i}{dt} - \frac{d\overline{q_i}}{dt}\right)q'_j q'_k}\right\}$$
$$= 3\left\{\overline{\frac{dq_i}{dt}q'_j q'_k} - \frac{dc_i}{dt}\overline{q'_j q'_k}\right\}$$
$$= 3\{L_{im}c_{mjk} + Q_{imn}(2c_m c_{njk} - c_{mn}c_{jk} + \overline{q'_m q'_n q'_j q'_k})\}$$
$$= \{3L_{im}c_{mjk} + 6Q_{imn}(c_m c_{njk} + c_{mj}c_{nk})\} - \frac{c_{ijk}}{\tau_d}. \quad (24)$$

In the final line of Eq. (24) a phenomenological eddy damping time scale τ_d has been introduced to model the neglect of the fourth cumulant [30,35]. CE2 is recovered in the limit $\tau_d \to 0$ as the third cumulant is suppressed in this limit. As τ_d is increased, contributions from the interactions of two fluctuations that produce another fluctuation begin to be felt. These nonlinear fluctuation + fluctuation → fluctuation interactions are dropped at order CE2, which retains only the fluctuation + fluctuation → mean and fluctuation + mean → fluctuation interactions [30]. This can be seen by examining Eqs. (21) and (22) and observing that the second cumulant only interacts through Q_{ijk} with the first cumulant, and not with itself. Upon increasing τ_d further, eventually realizability is lost as the second cumulant develops negative eigenvalues that are unphysical [30,36,37]. Furthermore, the appearance of a negative eigenvalue triggers an instability and the time-integrated EOMs diverge. We note that nonzero third cumulants are a mark of a non-Gaussian PDF for which all higher cumulants would generically be nonzero as well. Therefore, it is inconsistent to discard the fourth and higher cumulants, and that inconsistency makes itself felt in nonrealizability.

TABLE I. Comparison of the low-order statistically steady-state cumulants of the unforced Lorenz attractor ($\Gamma = 0$) as accumulated by DNS and as calculated with CE3. Modified Lorenz parameters are used (see Sec. II). Entries such as $O(10^{-4})$ indicate that these mean values are tending to zero as time averaging of DNS extends over increasing intervals of time.

Cumulant	DNS	CE3 ($\tau_d = 0.1$)	CE3 ($\tau_d = 0.5$)
$\overline{x}$	$O(10^{-4})$	0	0
$\overline{y}$	$O(10^{-4})$	0	0
$\overline{z}$	24.796	25.188	25.000
$\overline{x'x'}$	3.966	4.030	4.000
$\overline{x'y'}$	3.966	4.030	4.000
$\overline{x'z'}$	$O(10^{-5})$	0	0
$\overline{y'y'}$	5.395	4.392	4.908
$\overline{y'z'}$	$O(10^{-5})$	0	0
$\overline{z'z'}$	8.513	5.592	6.825

An appealing feature of cumulant expansions is that they respect the symmetries of the dynamical system. For instance, the CE3 fixed point exactly respects $\overline{x} = \overline{y} = 0$ due to the invariance of the Lorenz system under the reflection $\{x, y, z\} \to \{-x, -y, z\}$. This statistical symmetry is only approximately obeyed by DNS statistics accumulated over a finite time. Table I compares the first and second cumulants of the unforced Lorenz attractor as accumulated by DNS to those obtained from CE3 for two different choices of the time scale τ_d. Good qualitative agreement is found for both $\tau_d = 0.1$ and $\tau_d = 0.5$, demonstrating an insensitivity to the precise choice of the time scale. Table II displays the same cumulants, but now for the stochastically forced attractor. In addition, statistics obtained from the FPE zero mode are shown, calculated as the PDF-weighted sums of the desired variable over the domain of the lattice. Though the small stochastic forcing has a large

TABLE II. Same as in Table I but with added stochastic forcing ($\Gamma = 0.02$).

Cumulant	DNS	FPE	CE3 ($\tau_d = 0.1$)	CE3 ($\tau_d = 0.5$)
$\overline{x}$	$O(10^{-5})$	$O(10^{-9})$	0	0
$\overline{y}$	$O(10^{-5})$	$O(10^{-9})$	0	0
$\overline{z}$	24.834	24.834	25.192	25.004
$\overline{x'x'}$	3.977	3.978	4.034	4.004
$\overline{x'y'}$	3.971	3.972	4.031	4.001
$\overline{x'z'}$	$O(10^{-5})$	$O(10^{-8})$	0	0
$\overline{y'y'}$	5.350	5.349	4.396	4.912
$\overline{y'z'}$	$O(10^{-4})$	$O(10^{-8})$	0	0
$\overline{z'z'}$	8.150	8.135	5.610	6.829

effect on the fine structure of the PDF, it only changes the covariances slightly.

V. CONCLUSION

Direct statistical simulation is an attractive alternative to the accumulation of statistics by direct numerical simulation. Transforming the problem of finding the equal-time statistics of dynamical systems into a problem of sparse linear algebra offers an accurate and elegant alternative to traditional approaches. It would be interesting to employ a sparse preconditioner for the large nonsymmetric FPE operator studied here, as this should permit even higher resolutions to be reached, possibly revealing the fine ringlike steps in the Lorenz attractor PDF. Galerkin discretizations of the linear operator may also be interesting to explore.

We also showed that an expansion in equal-time cumulants closed at third order is able to reproduce the low-order statistics of the attractor, despite its highly nonlinear nature. The cumulant expansion technique is especially good for higher-dimensional systems due to its speed. Deterministic chaos and stochastic noise are seen to have similar effects on the low-order statistics [11,38] with both contributing to the variance. By contrast, Fig. 5 shows that the deterministic dynamics of the strange attractor produces high-order statistics that stochastic forcing erases.

ACKNOWLEDGMENTS

We are grateful to P. Zucker and D. Venturi for useful discussions. This research was supported in part by NSF Grants No. DMR-1306806 and No. CCF-1048701.

[1] R. F. Pawula, Approximation of the linear Boltzmann equation by the Fokker-Planck equation, Phys. Rev. **162**, 186 (1967).
[2] L. Pichler, A. Masud, and L. A. Bergman, *Computational Methods in Stochastic Dynamics* (Springer, Berlin, 2013), pp. 69–85.
[3] L. A. Bergman and B. F. Spencer, Jr., *Nonlinear Stochastic Mechanics* (Springer, Berlin, 1992), pp. 49–60.
[4] U. von Wagner and W. V. Wedig, On the calculation of stationary solutions of multi-dimensional Fokker-Planck equations by orthogonal functions, Nonlinear Dyn. **21**, 289 (2000).
[5] P. Kumar and S. Narayanan, Solution of Fokker-Planck equation by finite element and finite difference methods for nonlinear systems, Sadhana **31**, 445 (2006).
[6] A. Naess and B. K. Hegstad, Response statistics of van der Pol oscillators excited by white noise, Nonlinear Dyn. **5**, 287 (1994).
[7] E. N. Lorenz, Deterministic nonperiodic flow, J. Atmos. Sci. **20**, 130 (1963).
[8] I. Tikhonenkov, A. Vardi, J. R. Anglin, and D. Cohen, Minimal Fokker-Planck Theory for the Thermalization of Mesoscopic Subsystems, Phys. Rev. Lett. **110**, 050401 (2013).
[9] J. Thuburn, Climate sensitivities via a Fokker-Planck adjoint approach, Q. J. R. Meteor. Soc. **131**, 73 (2005).
[10] J. Gradišek, S. Siegert, R. Friedrich, and I. Grabec, Analysis of time series from stochastic processes, Phys. Rev. E **62**, 3146 (2000).
[11] S. Agarwal and J. S. Wettlaufer, Maximal stochastic transport in the Lorenz equations, Phys. Lett. A **380**, 142 (2016).
[12] J. M. Heninger, D. Lippolis, and P. Cvitanović, Neighborhoods of periodic orbits and the stationary distribution of a noisy chaotic system, Phys. Rev. E **92**, 062922 (2015).
[13] P. Kumar, S. Narayanan, S. Adhikari, and M. I. Friswell, Fokker-Planck equation analysis of randomly excited nonlinear energy harvester, J. Sound Vib. **333**, 2040 (2014).
[14] O. Ma and J. B. Marston, Exact equal time statistics of Orszag-McLaughlin dynamics investigated using the Hopf characteristic functional approach, J. Stat. Mech. (2005) P10007.
[15] D. K. Lilly, Numerical simulation of two-dimensional turbulence, Phys. Fluids **12**, II-240 (1969).
[16] J. Heninger, D. Lippolis, and P. Cvitanovic, Perturbation theory for the Fokker-Planck operator in chaos, arXiv:1602.03044.
[17] G. L. G. Sleijpen and H. A. Van der Vorst, A Jacobi-Davidson iteration method for linear eigenvalue problems, SIAM Rev. **42**, 267 (2000).
[18] D. R. Fokkema, G. L. G. Sleijpen, and H. A. Van der Vorst, Jacobi-Davidson Style QR and QZ algorithms for the reduction of matrix pencils, SIAM J. Sci. Comput. **20**, 94 (1998).
[19] A. B. Finnila, M. A. Gomez, C. Sebenik, C. Stenson, and J. D. Doll, Quantum annealing: A new method for minimizing multidimensional functions, Chem. Phys. Lett. **219**, 343 (1994).
[20] G. E. Santoro and E. Tosatti, Optimization using quantum mechanics: quantum annealing through adiabatic evolution, J. Phys. A **39**, R393 (2006).
[21] E. R. Davidson, The iterative calculation of a few of the lowest eigenvalues and corresponding eigenvectors of large real-symmetric matrices, J. Comput. Phys. **17**, 87 (1975).
[22] E. R. Davidson and W. J. Thompson, Monster matrices: Their eigenvalues and eigenvectors, Comput. Phys. **7**, 519 (1993).
[23] H. Risken, *The Fokker-Planck Equation: Methods of Solution and Applications* (Springer, Berlin, 1984).
[24] J. B. Marston, E. Conover, and T. Schneider, Statistics of an unstable barotropic jet from a cumulant expansion, J. Atmos. Sci. **65**, 1955 (2008).
[25] S. M. Tobias, K. Dagon, and J. B. Marston, Astrophysical fluid dynamics via direct statistical simulation, Astrophys. J. **727**, 127 (2011).
[26] S. M. Tobias and J. B. Marston, Direct Statistical Simulation of Out-of-Equilibrium Jets, Phys. Rev. Lett. **110**, 104502 (2013).
[27] J. B. Parker and J. A. Krommes, Zonal flow as pattern formation, Phys. Plasmas **20**, 100703 (2013).
[28] J. B. Parker and J. A. Krommes, Generation of zonal flows through symmetry breaking of statistical homogeneity, New J. Phys. **16**, 035006 (2014).
[29] J. Squire and A. Bhattacharjee, Statistical Simulation of the Magnetorotational Dynamo, Phys. Rev. Lett. **114**, 085002 (2015).
[30] J. B. Marston, W. Qi, and S. M. Tobias, Direct statistical simulation of a jet, arXiv:1412.0381.
[31] F. A. Chaalal, T. Schneider, B. Meyer, and J. B. Marston, Cumulant expansions for atmospheric flows, New J. Phys. **18**, 025019 (2016).

[32] N. A. Bakas and P. J. Ioannou, Emergence of Large Scale Structure in Barotropic β-plane turbulence, Phys. Rev. Lett. **110**, 224501 (2013).

[33] N. A. Bakas, N. C. Constantinou, and P. J. Ioannou, S3T stability of the homogeneous state of barotropic beta-plane turbulence, J. Atmos. Sci. **72**, 1689 (2015).

[34] U. Frisch, *Turbulence: The Legacy of A. N. Kolmogorov* (Cambridge University Press, Cambridge, 1995).

[35] S. A. Orszag, Lectures on the statistical theory of turbulence, in *Fluid Dynamics*, edited by R. Balian and J.-L. Peube, Proceedings of the Les Houches Summer School of Theoretical Physics (Gordon and Breach, London, 1977). pp. 235–374.

[36] R. H. Kraichnan, Realizability inequalities and closed moment equations, Ann. NY Acad. Sci. **357**, 37 (1980).

[37] P. Hänggi and P. Talkner, A remark on truncation schemes of cumulant hierarchies, J. Stat. Phys. **22**, 65 (1980).

[38] E. Knobloch, On the statistical dynamics of the Lorenz model, J. Stat. Phys. **20**, 695 (1979).